JCTC Journal of Chemical Theory and Computation

Article

pubs.acs.org/JCTC

Frozen-Orbital and Downfolding Calculations with Auxiliary-Field Quantum Monte Carlo

Wirawan Purwanto,* Shiwei Zhang,* and Henry Krakauer*

Department of Physics, College of William and Mary, Williamsburg, Virginia 23187-8795, United States

ABSTRACT: We describe the implementation of the frozen-orbital and downfolding approximations in the auxiliary-field quantum Monte Carlo (AFQMC) method. These approaches can provide significant computational savings, compared to fully correlating all of the electrons. While the many-body wave function is never explicit in AFQMC, its random walkers are Slater determinants, whose orbitals may be expressed in terms of any one-particle orbital basis. It is therefore straightforward to partition the full N-particle Hilbert space into active and inactive parts to implement the frozen-orbital method. In the frozen-core approximation, for example, the core electrons can be eliminated in the correlated part of the calculations, greatly increasing the computational efficiency, especially for heavy atoms. Scalar relativistic effects are easily included using the Douglas−Kroll−Hess theory. Using this method, we obtain a way to effectively eliminate the error due to single-projector, norm-conserving pseudopotentials in AFQMC. We also illustrate a generalization of the frozen-orbital approach that downfolds high-energy basis states to a physically relevant low-energy sector, which allows a systematic approach to produce realistic model Hamiltonians to further increase efficiency for extended systems.

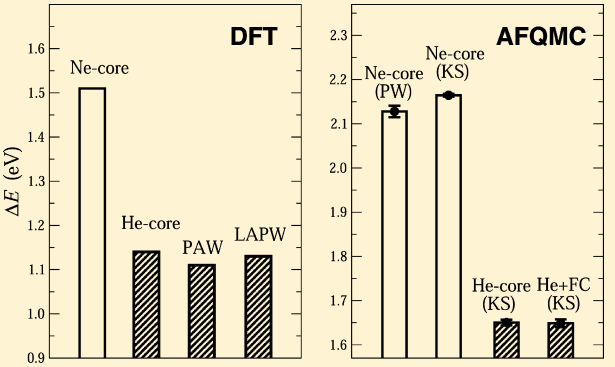

1. INTRODUCTION

Many-body methods such as quantum Monte Carlo (QMC) are capable of providing the most-accurate description of electronic systems from molecules to extended systems. Since these methods are significantly more expensive than traditional mean-field methods such as the density functional theory (DFT), it is highly desirable to find ways to economize many-body calculations without sacrificing their predictive power. Downfolding and partitioning methods have historically been used to develop effective Hamiltonians, where the nonessential degrees of freedom have been eliminated, so that key aspects of the correlated systems could be more easily studied. The Hubbard model exemplifies this approach, albeit being an extreme case, since it removes all materials-specific information.

Theories that partition the Hilbert space into physically important active and inactive subspaces are also well-developed for ab initio wavefunction-based, explicitly correlated many-body methods (see refs 1 and 2, for example). One of the most widely used examples of this partitioning is the familiar frozen-core (FC) approximation in quantum chemistry, where many-body wave functions are expanded as sums of Slater determinants with frozen core orbitals. This leads to a FC Hamiltonian, which acts only on the subspace spanned by canonical valence and virtual orbitals. Only the valence electrons are correlated, while the core−valence interactions appear as an effective one-body potential, thereby eliminating the core electrons from the calculation. Closely related valence-only pseudopotential (PP) Hamiltonians, whose accuracy is based on the validity of the FC approximation, also invoke this partitioning, but introduce additional approximations. Atomic PPs are usually constructed for reference atomic configurations and then used in many target systems. The accuracy (transferability) of the PP across many target systems must then be determined a posteriori. In addition, most PPs used in QMC calculations are of the single-projector (one per angular momentum channel), norm-conserving type. This type of PP can introduce an uncontrollable systematic bias in QMC calculations, which becomes more severe in extended systems.[3−7] To date, a satisfactory solution to this problem has not been found. In contrast, the FC Hamiltonian is obtained specifically for the target system, using canonical orbitals from a lower level of theory such as the Hartree−Fock (HF) orbitals, or natural orbitals obtained from a configuration interaction (CI) or a second-order Møller−Plesset perturbation theory calculation. This eliminates the additional algorithmic layer of constructing norm-conserving PPs.

It is possible to generalize the frozen orbital approach to other ways of partitioning the Hilbert space into active and inactive regions. In molecular and condensed matter physics, for example, the active region may sometimes be identified spatially, corresponding to a localized region where strong electron correlation effects affect a relatively small number of atoms, while the bulk of the system can be treated with a lower level of theory. This provides opportunities for generating realistic, material-specific model Hamiltonians whose many-body treatment will be simpler than the full Hamiltonian but

Received: July 23, 2013

dx.doi.org/10.1021/ct4006486 | J. Chem. Theory Comput. XXXX, XXX, XXX−XXX

which can retain the essential correlation effects quantitatively in a systematic manner.

In this paper, we develop and demonstrate a method to perform PP-free QMC calculations in both molecular and extended systems. In molecular systems, this is equal to the traditional FC approximation; in extended (solid) systems, however, a downfolding method is employed in conjunction with the FC approximation to achieve PP-free calculations. In solids, our approach provides a simple way to obtain a many-body Hamiltonian whose accuracy is systematically improvable and which can be used in any quantum chemistry method. The basis sets and matrix elements correctly encode the Coulomb interaction and the periodicity, and allow any twist angle for the supercell. We show how downfolding and frozen orbital approaches can be implemented in the auxiliary-field quantum Monte Carlo (AFQMC) method[3,8,9] to gain significant computational savings compared to fully correlating all the electrons.

AFQMC is a many-body method applied in condensed matter physics, quantum chemistry, and nuclear physics. AFQMC stochastically samples the many-body wave function to obtain observables such as the ground-state energy of a system. Like other QMC methods, this leads to a modest polynomial scaling [$O(M^3)$ or $O(M^4)$] as the system size is increased, rather than exponential scaling of CI calculations, or high-order polynomial scaling of typical quantum chemistry many-body methods. AFQMC with the phaseless approximation[8] has demonstrated high accuracy in applications to many molecular and extended systems.[9−13] AFQMC is based on random walks in the space of Slater determinants, where each random walker is a full Slater determinant expressed with respect to a chosen one-particle basis set. Most AFQMC applications to date have used planewaves for extended systems and Gaussian-type orbitals (GTO) for atoms and molecules. In this paper, we show that the ability of AFQMC to sample explicit Slater determinants and to use *any* one-particle basis can be exploited to implement various partitioning and downfolding schemes.

The paper is organized as follows: section 2 presents the implementation of the frozen orbital approximation after first reviewing pertinent aspects of the phaseless AFQMC method. Section 3 benchmarks the frozen orbital implementation in AFQMC against exact results in small GTO basis and against experimental results for large, realistic basis sets. In section 4, we demonstrate an application of the downfolding method to eliminate errors from the use of standard norm-conserving PPs. Section 5 summarizes our results and discusses the prospects of the new frozen orbital capability in AFQMC.

2. FROZEN ORBITAL METHOD IN AFQMC

AFQMC is an explicitly many-body method for a system of N interacting particles. The focus here will be on the electronic Hamiltonian for real materials. Since AFQMC is conveniently formulated in second-quantized form, however, the methods described in this paper can be directly used to treat any Hamiltonian with one- and two-body interactions.

2.1. Hamiltonian. The Hamiltonian is given by

$$\begin{aligned}\hat{H} &= \hat{K} + \hat{V} \\ &= \sum_{\mu\nu} K_{\mu\nu} c_\mu^\dagger c_\nu + \frac{1}{2}\sum_{\mu\nu\lambda\rho} V_{\mu\nu\lambda\rho} c_\mu^\dagger c_\nu^\dagger c_\lambda c_\rho\end{aligned} \tag{1}$$

where the lower case Greek indices run over a chosen finite set of M orthonormal single-particle basis functions; $\hat{K}$ and $\hat{V}$ denote the one- and two-electron interactions, respectively; and $c_\mu^\dagger$ and c_μ are the creation and destruction operators, respectively. This form encompasses all of the orbital-based standard approaches for interacting electron systems, from real materials (with all-electron, PP, or FC treatments) to effective Hamiltonian models (with lattice-based treatments, such as the Hubbard model, and other downfolded models with reduced degrees of freedom). Any N-electron fermionic state Ψ can be expressed as a linear combination of Slater determinants $|\phi\rangle = \hat{\phi}_1^\dagger\hat{\phi}_2^\dagger...\hat{\phi}_N^\dagger|0\rangle$ with their respective weights a_ϕ:

$$|\Psi\rangle = \sum_\phi a_\phi |\phi\rangle \tag{2}$$

where $\hat{\phi}_i^\dagger = \sum_\mu \phi_{\mu i} c_\mu^\dagger$. The number of determinants in this expansion increases exponentially as a function of N and M. An exact, explicit solution of the N-electron Hamiltonian is therefore not possible, except for small systems. AFQMC achieves polynomial scaling by using stochastic methods with importance sampling, as discussed next.

2.2. AFQMC Ground-State Projection, Importance Sampling, and Phaseless Approximation. This section reviews key elements of AFQMC, which are needed to discuss our implementation of the frozen orbital approximation. AFQMC finds the ground-state energy E_0, using a mixed estimator and imaginary-time projection from a trial wavefunction Ψ_T:

$$E_0 = \frac{\langle\Psi_T|\hat{H}|\Psi_0\rangle}{\langle\Psi_T|\Psi_0\rangle} = \lim_{\beta\to\infty}\frac{\langle\Psi_T|\hat{H}e^{-\beta\hat{H}}|\Psi_T\rangle}{\langle\Psi_T|e^{-\beta\hat{H}}|\Psi_T\rangle} \tag{3}$$

where Ψ_0 is the exact ground state, and Ψ_T is assumed to be nonorthogonal to Ψ_0. The projection in eq 3 is cast into the form of a branching random walk with Slater determinants $|\phi\rangle$, using iterations with a small time step $\tau \to 0$,

$$\lim_{\beta\to\infty} e^{-\beta\hat{H}}|\Psi_T\rangle \approx e^{-\tau\hat{H}}e^{-\tau\hat{H}}\cdots e^{-\tau\hat{H}}|\Psi_T\rangle \to |\Psi_0\rangle \tag{4}$$

The small imaginary time step τ allows a Trotter−Suzuki breakup of the exponential operator,

$$e^{-\tau\hat{H}} \approx e^{-\tau\hat{K}/2}e^{-\tau\hat{V}}e^{-\tau\hat{K}/2} + O(\tau^3) \tag{5}$$

After a Hubbard−Stratonovich transformation of $e^{-\tau\hat{V}}$, the projection operator can then be expressed as a high-dimensional integral over auxiliary fields $\boldsymbol{\sigma}$,[8,14]

$$e^{-\tau\hat{H}} = \int d\boldsymbol{\sigma} P(\boldsymbol{\sigma}) e^{-\tau\hat{K}/2}e^{\sqrt{\tau}\boldsymbol{\sigma}\cdot\hat{\mathbf{v}}}e^{-\tau\hat{K}/2} \tag{6}$$

where $P(\boldsymbol{\sigma})$ is the normal distribution function, $\hat{\mathbf{v}}$ is a set of one-body operators, and the operator in the integrand, acting on a Slater determinant, simply yields another determinant,

$$e^{-\tau\hat{K}/2}e^{\sqrt{\tau}\boldsymbol{\sigma}\cdot\hat{\mathbf{v}}}e^{-\tau\hat{K}/2}|\phi\rangle \equiv e^{-\tau\hat{h}(\boldsymbol{\sigma})}|\phi\rangle \to |\phi'\rangle \tag{7}$$

Starting with an initial population of walkers (which are usually set equal to Ψ_T), the mixed estimator in eq 3 is then stochastically sampled. As the one-body operator $\hat{h}(\boldsymbol{\sigma})$ is generally complex, however, the orbitals in $|\phi\rangle$ will become complex as the projection proceeds, and the statistical fluctuations in the mixed estimator increase exponentially with projection time. To control this problem, a phaseless

dx.doi.org/10.1021/ct4006486 | J. Chem. Theory Comput. XXXX, XXX, XXX−XXX

approximation was introduced[8] based on the complex importance function $\langle \Psi_T|\phi\rangle$. After the importance sampling transformation, eq 7 becomes

$$e^{-\tau\hat{K}/2}e^{\sqrt{\tau}(\bar{\sigma}-\bar{\sigma}[\phi])\cdot\hat{\mathbf{v}}}e^{-\tau\hat{K}/2}|\phi\rangle \rightarrow |\phi'\rangle \tag{8}$$

where the "force bias" $\bar{\sigma}[\phi]$ is given by

$$\bar{\sigma}[\phi] \equiv -\sqrt{\tau}\frac{\langle \Psi_T|\hat{\mathbf{v}}|\phi\rangle}{\langle \Psi_T|\phi\rangle} \tag{9}$$

The mixed estimator at each time slice becomes a weighted sum over the walkers

$$E_0 \approx \frac{\sum_\phi w_\phi E_L[\phi]}{\sum_\phi w_\phi} \tag{10}$$

where $E_L[\phi]$ is the "local energy" of each walker, which is defined as

$$E_L[\phi] \equiv \frac{\langle \Psi_T|\hat{H}|\phi\rangle}{\langle \Psi_T|\phi\rangle} \tag{11}$$

and its weight w_ϕ is accumulated over the random walk, as described in more detail in refs 3, 8, 9, and 15.

2.3. AFQMC Implementation of the Frozen Orbital Method. It is often useful to partition the N-electron Hilbert space into active ($\mathbb{A}$) and inactive ($\mathbb{I}$) parts, reflecting physical considerations based on energetic, spatial, or other factors. Since AFQMC is an orbital-based method, this partitioning is facilitated by the freedom to use *any* orthonormal basis in eqs 1 and 2. By definition, electrons in the $\mathbb{I}$ space are constrained to occupy, in the mean-field sense, the orbitals defined by a lower-level of theory, such as the canonical orbitals in HF, DFT, or natural orbitals determined from an approximate CI calculation. This implicitly imposes an orthogonality constraint on the $\mathbb{A}$-space orbitals.

The AFQMC formalism outlined in the previous section will need to be modified to implement this approach. The $\mathbb{I}$ orbitals in the AFQMC determinants (eq 2) should be frozen during the random walks, and orthogonality conditions should be imposed, for numerical stability, on the active electrons. In addition, the HS operators $\hat{\mathbf{v}}$ must be modified to act only in the $\mathbb{A}$ sector of the N-electron Hilbert space, and only the $\mathbb{A}$ orbitals should appear in the force bias $\bar{\sigma}[\phi]$ in eq 9.

An alternative and perhaps more elegant approach is to define a frozen-orbital Hamiltonian $\hat{H}_\mathbb{A}$ that acts only on the $\mathbb{A}$ sector of the Hilbert space. The goal is to have the $\mathbb{I}$ orbitals appear explicitly, if at all, only in one-body operators acting on the $\mathbb{A}$ space. (They do not appear, for example, in the effective core potential or norm-conserving PP formulations.) The derivation of $\hat{H}_\mathbb{A}$ proceeds from a separability approximation of the many-body wavefunction:

$$\Psi \approx \mathcal{A}(\Psi_\mathbb{I}\Psi_\mathbb{A}) \tag{12}$$

where the wavefunctions $\Psi_\mathbb{I}$ and $\Psi_\mathbb{A}$ are assumed to be mutually orthogonal and individually antisymmetrized and normalized. The antisymmetrizer $\mathcal{A}$ permutes electrons between $\Psi_\mathbb{I}$ and $\Psi_\mathbb{A}$. This separation allows the energy of the total system to be effectively mapped onto an equivalent system involving only the $\mathbb{A}$ electrons:

$$E = \langle \Psi|\hat{H}|\Psi\rangle = \langle \Psi_\mathbb{A}|\hat{H}_\mathbb{A}|\Psi_\mathbb{A}\rangle \tag{13}$$

where the frozen orbital Hamiltonian $\hat{H}\hat{H}_\mathbb{A}$ is given by[1,2]

$$\hat{H}_\mathbb{A} = \sum_{ij\in\mathbb{A}} K_{ij}c_i^\dagger c_j + \frac{1}{2}\sum_{ijkl\in\mathbb{A}} V_{ijkl}c_i^\dagger c_j^\dagger c_k c_l + \sum_{ij\in\mathbb{A}} V_{ij}^{\mathbb{I}-\mathbb{A}}c_i^\dagger c_j + E^\mathbb{I} \tag{14}$$

The first term includes the kinetic energy and all one-body external potentials acting on the $\mathbb{A}$ electrons, and the second term includes the two-body Coulomb interactions among them. The third term is a one-body interaction that represents the interaction between the inactive and active orbitals. It includes Coulomb and exchange interactions between the $\mathbb{A}$ and $\mathbb{I}$ electrons; it is formally identical to a nonlocal PP. The fourth term is a constant energy, which represents all interactions among the $\mathbb{I}$ electrons. (If HF is used as the low level theory, $E^\mathbb{I}$ has the form corresponding to a closed-shell determinantal wavefunction of the $\mathbb{I}$ electrons.[2])

As a result of the mapping defined by eqs 13 and 14, all of the AFQMC formalism described in Section 2.2 can be immediately applied. Thus, the local energy, with $\hat{H} \rightarrow \hat{H}_\mathbb{A}$ in eq 11, is evaluated using a trial wave function Ψ_T and random walkers ϕ, both of which now depend only on the $\mathbb{A}$ electrons and orbitals. Similarly, the force bias $\bar{\sigma}$ in eq 9 is evaluated using HS one-body operators $\hat{\mathbf{v}}$ that are obtained only from the two-body $\mathbb{A}$-space V_{ijkl} matrix elements in eq 14.

In the FC applications to atoms and molecules with GTO basis (section 3), we use the conventional partitioning provided naturally by the restricted closed- or open-shell HF orbitals of the system being studied. The HF core orbitals defines the $\mathbb{I}$-space, and eq 14 is expressed in the basis of the valence and virtual orbitals. In our calculations, we have sometimes used other types of wavefunctions as Ψ_T, such as the DFT, unrestricted HF (UHF), or the complete active space self-consistent field (CASSCF) wavefunctions. For the FC approximation to be valid, the calculation results should be insensitive to the small variations in the $\mathbb{A}-\mathbb{I}$ partitioning defined by the core orbitals of these wavefunctions. We find that this holds true for our calculations. Substituting the UHF or CASSCF wavefunction core orbitals with those from HF results in only small changes (~3 meV) in the total energy, which is negligible for our purposes.

In the downfolding applications (section 4), the single-particle basis consists of the eigenstates from a DFT band structure calculation. As described later, a simple truncation scheme is introduced, which will systematically converge the basis set to the full basis limit (which is just a unitary transformation from the original planewave basis). In the case of spin-polarized DFT calculations, where the spin-up and down electrons can have different spatial orbitals, we choose to use the majority-spin orbitals as the basis functions for both spin sectors. Additional errors introduced by this choice can thus be considered as a part of the basis truncation error, which vanishes in the limit of full basis.

3. BENCHMARKING FROZEN ORBITAL AFQMC: FROZEN-CORE CALCULATIONS FOR ATOMS AND MOLECULES

In QMC calculations, a satisfactory treatment of core electrons has not been realized, despite the absolute necessity of using some form of a PP as calculations move toward heavier elements and ever larger scales. The most commonly used form is atomic pseudopotentials, which are usually constructed for

dx.doi.org/10.1021/ct4006486 | J. Chem. Theory Comput. XXXX, XXX, XXX−XXX

reference atomic configurations. The transferability of the PP across many target systems is challenging to determine, and systematic accuracy can be difficult to achieve. In addition, most PPs used in QMC calculations are of the single-projector (one per angular momentum channel), norm-conserving type, which tends to further limit transferability. The frozen-core approach offers a significant step forward. It retains all the advantages of using PPs, namely, the reduction of system size by eliminating core electrons, the change of energy scale and hence the reduction of statistical and time-step errors, while allowing much better transferability. The FC Hamiltonian is obtained for each target system, using canonical orbitals from a lower level of theory, with no additional algorithmic layers.

The AFQMC frozen-orbital implementation is first tested by comparisons with standard quantum chemistry methods for atoms and small molecules, using GTO basis sets. We compare with full configuration interaction (FCI) calculations, which are feasible for small systems. This constitutes a rigorous test of our methodology, since both AFQMC and FCI use the same underlying FC Hamiltonian (eq 14), expressed in the basis of the orthonormal HF valence and virtual orbitals. Using larger basis sets, we also calculate ionization potentials for the transition-metal atoms Co and Zn and compare to experimental values.

3.1. Total Energy Comparisons with Exact Results. Table 1 compares AFQMC total energies with exact results for some atoms and molecules. In Be, HF, and Li_2, only the 1s states of the Be, F, and Li atoms are frozen, while in Zn and Zn^+, core states through the 3p shell are frozen, for a total of nine inactive orbitals. For most of the systems, AFQMC results were obtained using single-determinant HF Ψ_T. Multideterminant Ψ_T derived from CASSCF were also used in some cases for comparison. The Hamiltonian matrix elements and HF wave functions were generated using a modified NWCHEM[16] code. The CASSCF wave functions were generated using either the NWCHEM or GAMESS[17] quantum chemistry package. GAMESS is used to calculate the FCI energies.

Table 1. Total Energies (Hartree Atomic Units) for Several Atoms and Small Molecules[a]

	basis set	M_c	Ψ_T	AFQMC	FCI
Be	6-31G*	1	HF	−14.6116(2)	−14.6134
Be	6-31G*	1	CASSCF	−14.61361(1)	
Li_2	cc-pVDZ	2	HF	−14.9017(1)	−14.9005
HF	cc-pVDZ	1	HF	−100.2020(1)	−100.2011
Zn	6-31G	9	HF	−1777.6771(2)	−1777.6774
Zn	6-31G	9	CASSCF	−1777.6775(5)	
Zn^+	6-31G	9	HF	−1777.3705(4)	−1777.3700
Zn^+	6-31G	9	CASSCF	−1777.3706(5)	

[a]FC AFQMC results are compared with exact values from FCI. The AFQMC statistical error bars are on the last digit and are indicated in parentheses. The basis sets and the number of FC orbitals (M_c) are indicated. Ψ_T is the trial wave functions used in AFQMC.

The AFQMC energies in Table 1 are in good agreement with the exact results. Those using a single determinant HF Ψ_T have systematic errors typically less than ∼1 mHa (0.0272 eV), well within chemical accuracy. The largest discrepancy for HF Ψ_T occurs in Be, ∼2 mHa. This is because of the near-degeneracy of the 2s and 2p levels in the Be atom. Using a CASSCF Ψ_T of four determinants brings the calculated AFQMC energy to within only 0.2 mHa of FCI. For Zn and Zn^+, the AFQMC results are insensitive to the Ψ_T used.

3.2. Transition-Metal Atom Ionization Potentials: Comparison with Experimental Results. We now benchmark the FC AFQMC in realistic calculations using large basis sets. With this formalism, scalar relativistic effects are included straightforwardly in the Hamiltonian using the Douglas−Kroll−Hess (DKH) approximation.[19−21] We compare the ionization potentials (IPs) for cobalt and zinc with experiment in Table 2.

Table 2. Ionization Potentials of Co and Zn Computed Using FC AFQMC, Compared with Experimental Results[a]

	Ionization Potential (in eV)	
	cobalt	zinc
HF	8.30	7.79
CCSD(T)	7.89	9.37
AFQMC/HF	7.73(4)	9.47(6)
AFQMC/CASSCF	7.80(4)	9.43(4)
Expt.	7.87	9.39

[a]AFQMC results are shown using two different trial wavefunctions: HF and CASSCF. For comparison, HF and CCSD(T) results are also shown. All calculated results have been extrapolated to the complete basis set limit, as described in the text. The final AFQMC statistical error bars are on the last digit and are shown in parentheses. Experimental results have been adjusted to remove spin-orbit effects (see ref 18).

In cobalt, both the atomic and singly ionized ground states have partially filled d-shell configurations ($3d^74s^2$ and $3d^84s^0$, respectively); while both Zn and Zn^+ atom have a completely filled $3d^{10}$ shell as well as spherical $4s^2$ and $4s^1$ configurations, respectively. These atoms thus represent a spectrum of transition-metal character. Unlike the zinc calculations in Table 1, which are small systems to compare with exact results, we use a small frozen core in the calculations here. Only the innermost 1s, 2s, and 2p core states are frozen (five inactive orbitals). The use of a small core allows the 3s and 3p electrons to be fully correlated along with the 3d electrons, which is important for accurate results, since the radial extent of the 3s, 3p, and 3d orbitals are similar. The use of large, relativistic GTO basis sets[18] is crucial to achieve systematic extrapolation[12,22] of the calculated results to the complete basis set (CBS) limit. [We used triple- and quadrupole-zeta correlation consistent core−valence basis sets (cc-pwCVxZ-DK with x = 3, 4), which were designed for use with the DK scalar-relativistic treatment.] The multideterminant Ψ_T used in the AFQMC/CASSCF calculations typically consists of ∼10−40 determinants; they are obtained by taking the ones with the largest weights, and they account for ≳99% of the total weight of the full CASSCF wavefunction.[10,23,24] We have verified the quality of the CASSCF Ψ_T by increasing the size of the active space in the CASSCF calculation and ensuring that the AFQMC energies with different CASSCF trial wavefunctions do not change significantly.

Calculated IP results from AFQMC, extrapolated to the CBS limit, are shown in Table 2. Also shown are the corresponding results from the coupled-cluster singles and doubles and perturbative triples [CCSD(T)] method. The AFQMC/CASSCF results are seen to be in excellent agreement with experiment, as are the CCSD(T) values. The benchmark results demonstrate the accuracy of FC AFQMC to be comparable to the best FC quantum chemistry methods, consistent with

earlier results from many all-electron or ECP calculations.[9,10,12,23] Using the HF trial wavefunction, the AFQMC/HF values are as good for zinc but slightly worse for cobalt. This can be traced to the Co^+ mean-field HF solution, which predicts an incorrect ground state, quintuplet $3d^7\ 4s^1$, rather than tripet $3d^8\ 4s^0$. As seen in the table, the Co ionization potential is overestimated at the HF level.

4. BASIS DOWNFOLDING AND PSEUDOPOTENTIAL-FREE AFQMC CALCULATIONS IN SOLIDS

In this section, we discuss a more general application of the frozen-orbital method in extended systems, where the broader aim is to greatly reduce the relevant degrees of freedom and/or the number of explicitly correlated electrons. We present an example, using the frozen orbital approximation, to replace high-energy planewave basis states in favor of a more compact representation of lower-energy basis functions. Since the downfolding and generation of one- and two-body matrix elements are done at the mean-field level, the approach also affords the opportunity to eliminate most of the errors associated with the PP in the subsequent many-body calculations, as we describe below. This idea is related to the downfolding method, which focuses on the low-energy, physically relevant, sector of the Hilbert space, while downfolding high-energy states to obtain an effective Hamiltonian that acts only in the low-energy subspace.

Planewave basis sets are commonly used to describe extended systems. Calculations using a planewave basis are appealing because the basis is complete and convergence to the CBS limit is straightforward, using only a single cutoff energy parameter E_{cut}. However, planewave basis sets can be inefficient. Since the basis is unbiased and does not build in information about the specific system being studied, large basis sets may be required ($>10^4$ planewaves), especially in supercell calculations. Basis sets constructed from localized orbitals, on the other hand, can be tailored to the physics of a particular system, although convergence to the CBS limit is not as straightforward. There are many possible choices for a local orbital basis, including Wannier functions, GTO, Slater-type orbitals, or numerical basis sets.

For the present application, we choose a simple transformation from the planewave basis $\{|\mathbf{G}\rangle\}$ to the basis of Kohn−Sham (KS) orbitals $\{|\chi_i\rangle\}$, where $|\chi_i\rangle \equiv \sum_{\mathbf{G}} \chi_i(\mathbf{G})|\mathbf{G}\rangle$ is obtained by self-consistently solving the KS Hamiltonian,

$$\sum_{\mathrm{G}'} H_{\mathrm{KS}}[\rho](\mathbf{G}, \mathbf{G}')\chi_i(\mathbf{G}') = \varepsilon_i \chi_i(\mathbf{G}) \tag{15}$$

computed at a single Bloch vector $\mathbf{k}$. The associated KS band energies (ε_i) are used to truncate the new basis according to a specified energy cutoff ($\varepsilon_i < \varepsilon_{\max}$), resulting in $N_{\mathrm{KS}} \ll 10^4$ basis functions. This basis is systematically improvable by increasing the band cutoff $\varepsilon_{\max}$; in the limit of including all bands, it is simply a unitary transformation from the full planewave basis. For certain applications, involving similar atomic arrangements, where favorable cancellation of errors may be expected, this straightforward approach can lead to significant savings. Other possible choices for the target basis $\{|\chi_i\rangle\}$, such as Wannier functions, projected atomic orbitals, etc., are likely to be more efficient in certain situations, but the simple approach above is sufficient to illustrate the basic concept.

The following describes the practical steps we used to construct the second-quantized Hamiltonian in the KS basis. Let the Hamiltonian matrix elements in the planewave basis be denoted by

$$K_{\mathrm{G,G}'} \equiv \langle \mathrm{G}|\hat{K}|\mathrm{G}'\rangle \tag{16}$$

and

$$V_{\mathbf{GG}',\mathbf{G}''\mathbf{G}'''} \equiv \langle \mathbf{GG}'|\hat{V}|\mathbf{G}'''\mathbf{G}''\rangle \tag{17}$$

respectively, for the one-body and two-body terms. These matrix elements are simple functions and are straightforward to compute in the planewave basis. The one-body Hamiltonian in the downfolded basis is given by

$$K_{ij} \equiv \sum_{\mathbf{GG}'} \chi_i^*(\mathbf{G}) K_{\mathbf{G,G}'} \chi_j(\mathbf{G}') \tag{18}$$

which is inexpensive to compute. The two-body Hamiltonian in the downfolded basis is formally given by

$$V_{ijkl} \equiv \sum_{\mathbf{GG}''\mathbf{G}'''} \chi_i^*(\mathbf{G})\chi_j^*(\mathbf{G}')V_{\mathbf{GG}',\mathbf{G}''\mathbf{G}'''}\chi_l(\mathbf{G}''')\chi_k(\mathbf{G}'') \tag{19}$$

Fast Fourier transform (FFT) can be used to evaluate eq 19 efficiently. Significant computational and memory savings are further achieved by employing a modified Cholesky decomposition (mCD) procedure,[12,25−27]

$$V_{ijkl} \equiv V_{(il),(kj)} = \sum_{\gamma} L_{(il)}^{\gamma} L_{(kj)}^{\gamma *} + O(\delta) \tag{20}$$

to represent the two-body Hamiltonian matrix. [Note that, unlike the mCD procedure with GTO basis sets, the order of the second compound index, (kj), is reversed in eq 20, because the basis functions generally are complex-valued.] Basis downfolding defined by eqs 18 and 19 applies, regardless of the use of PP or FC approximation. When this downfolding is combined with the FC approximation to freeze the core degrees of freedom, we obtain a PP-free Hamiltonian for extended systems, as will be demonstrated in the latter part of this paper. Errors from finite-size simulation cells can be corrected by applying "twist averaging" over a sampling of Bloch vectors[28] and an a posteriori correction using the finite-size DFT exchange-correlation functionals.[29,30]

We first illustrate the convergence behavior of the KS basis by calculating the spin gap in bulk silicon. A primitive cell is considered at a single $\mathbf{k}$-point (Baldereschi[31]). Using each set of truncated KS orbitals as the basis set, we construct the Hamiltonian in eq 1 and calculate the AFQMC energy. We increase the number of the KS orbitals (N_{KS}) until it reaches the full number of planewaves. These calculations are operationally equivalent to AFQMC with a GTO basis;[9] all information about the structure and periodicity of the cell is reflected only in the values of the matrix elements. The results are shown in Figure 1 and compared with the full planewave results, which are obtained with planewave-AFQMC calculations.[3,11] The DFT and planewave AFQMC calculations used a norm-conserving PP with a planewave cutoff of 12.25 Ry; the KS-basis AFQMC does not employ the FC approximation in this test, treating all the valence electrons as defined by DFT. The total energies and the spin gap converge to the full planewave limit, as expected. The total energies shows a slow, monotonic convergence behavior as a function of N_{KS}.

dx.doi.org/10.1021/ct4006486 | J. Chem. Theory Comput. XXXX, XXX, XXX−XXX

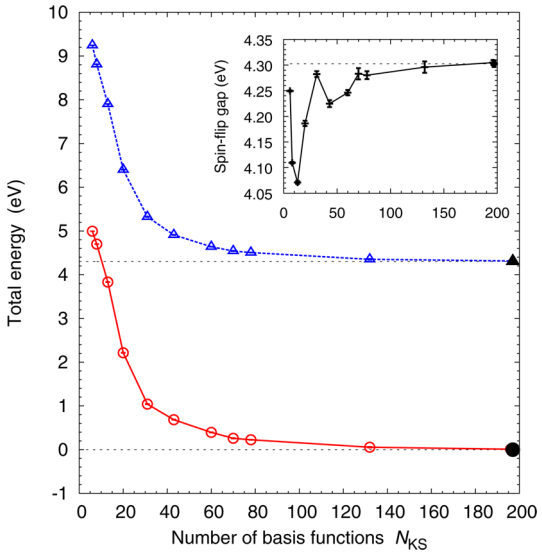

Figure 1. Convergence of the AFQMC total energies and spin gap, each as a function of the number of KS bands (N_{KS}). Total energies of the ground (excited/spin-flip) state in the silicon primitive cell are shown as open circles (triangles), respectively. The filled symbols denote the planewave AFQMC results. Total energies are shifted such that the planewave AFQMC ground-state energy is zero. Shown in the inset is the corresponding spin gap. QMC statistical error bars are much smaller than the symbol size.

However, the spin-flip gap computed using the KS basis is much closer to the planewave gap, even with a small number of KS bands. For example, at $N_{KS} \approx 40$, the total energy is almost 1 eV away from the basis set limit, but the gap is only ~0.07 eV away. The convergence of the gap is not monotonic as a function of N_{KS}.

We next apply the downfolding technique to a more-correlated extended system, the crystalline MnO. We will demonstrate that the method provides a treatment of a strongly correlated system using a realistic model Hamiltonian, free of PP errors. As a simple prototype for Mott insulators, MnO poses a major challenge for theoretical methods, with the presence of localized 3d electrons. At ambient temperatures and pressures, MnO chemically orders in a rocksalt crystal structure. At temperatures of <118 K,[32] an antiferromagnetic ordering (type-II AFM) sets in, accompanying rhombohedral distortion of the crystal. High-pressure experiments[32,33] have presented evidence of a simultaneous structural and magnetic phase transition. At ~105 GPa, the crystal volume collapses by ~20%, accompanied by a local magnetic moment collapse. Various DFT calculations yield varying predictions for the nature of the transition,[34] with different values of the transition pressure and whether the transition is from metal to insulator.

We use the primitive rocksalt MnO unit cell with periodic boundary conditions as the model system to compute the high-spin to low-spin state vertical energy gap. As the primitive cell contains an odd number of electrons, we represent the low-spin state by the $S = 1/2$ state and the ferromagnetic phase by the $S = 5/2$ state. The spin gap is computed as

$$\Delta E \equiv E_{S=1/2} - E_{S=5/2} \tag{21}$$

All calculations were done near the experimental volume, corresponding to a rocksalt cubic lattice constant of $a = 8.4$ Å. Both the DFT and QMC calculations were done at the L-point in the Brillouin zone. We have chosen a small simulation cell here, so that high-resolution calculations can be easily done. Our goal is thus not to compare with experiment or other theoretical results, but rather to study the accuracy of the downfolded many-body Hamiltonian as a function of band cutoff, comparing to AFQMC results using the full planewave basis.

A secondary goal of this work is to show how the frozen-core approach combined with downfolding can largely remove the error from the use of conventional norm-conserving PPs. As discussed earlier, this error poses a significant problem in QMC calculations. In systems containing 3d transition-metal atoms, for example, relatively hard PPs are typically constructed such that the semicore 3s and 3p states are included as valence states (Ne-core PP), which is especially important for the early 3d atoms. Nevertheless, Ne-core PPs have been found to introduce unsatisfactorily large errors.[7] We show below that, this problem can be largely ameliorated with our approach. A He-core PP (retaining the 2s and 2p as valence states) is used for the transition-metal atom to generate the KS basis set. In the subsequent AFQMC calculations with the downfolded Hamiltonian, the 2s and 2p states are treated with the FC approximation, freezing them at the DFT level using the orbitals derived from the solid, rather than from an atomic calculation.

The PP DFT calculations were done with the ABINIT[35] package, using the generalized gradient Perdew–Becke–Ernzerhof exchange-correlation functional; PWSCF[36] was used for the projector augmented wave (PAW) calculations; all-electron linearized augmented planewave (LAPW) calculations were done with ELK.[37] All our norm-conserving PPs assume the Kleinman–Bylander (KB) form, and were generated using the OPIUM package.[38] A standard norm-conserving He-core PP is used for the O atoms. [The O PP was generated with the following parameters: r_c = 1.1 au for the s and p channels, with the s channel being the local projector.] Both Ne- and He-core Mn PPs used a single-projector for each angular momentum channel (as is almost universally done for norm-conserving PPs) and were designed for planewave cutoffs of 100 and 1600 Ry, respectively. [The Ne-core Mn PP has r_c values of 1.15, 1.15, 1.5 au for the s, p, and d channels (using the p-channel as the local projector). The He-core Mn PP has r_c values of 0.36, 0.305, and 0.5 au for the s, p, and d channels (using the s-channel as the local projector). Scalar relativity is included in the construction of both PPs.] Direct use of He-core PPs in QMC is costly because of the hardness of the PP (exceedingly high cutoff), and is almost never done (although multiple-projector norm-conserving PPs, or even the more accurate PAW, could be implemented in AFQMC). The same number of KS orbitals were used for both the low- and high-spin states.

Figure 2 shows the convergence of the spin-gap ΔE with respect to N_{KS}. These calculations were done with the Ne-core PP. The spin gap value from the full planewave basis AFQMC is also shown. The graph shows the spin gaps computed in two slightly different downfolding approaches. In the first approach ("separate KS basis"), the KS basis used in AFQMC is constructed from the corresponding DFT calculation for each magnetic state. This results in different downfolded Hilbert spaces for the two calculations, which have different convergence rates to the full planewave basis limit. In the second approach ("uniform KS basis"), only one KS basis is used in AFQMC calculations for all the magnetic states; in this case, we expand all the Hamiltonians and wave functions in

dx.doi.org/10.1021/ct4006486 | J. Chem. Theory Comput. XXXX, XXX, XXX–XXX

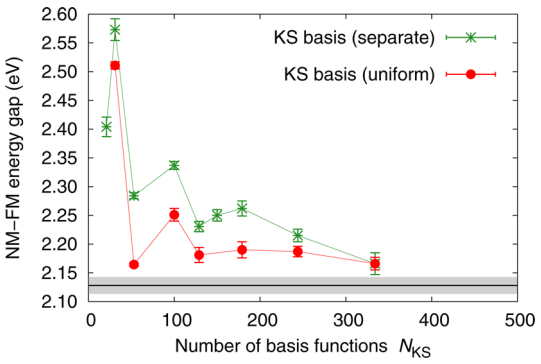

Figure 2. Convergence of the AFQMC high-low spin gap in MnO as a function of N_{KS}. The KS gaps are shown as points with the statistical error bars; lines are only present to aid the eye. The two curves correspond to two different approaches in defining the truncated KS basis, as described in the text. The energy gap from the full planewave AFQMC calculation is shown as a solid black horizontal line with the gray shading representing its statistical error.

terms of the majority-spin KS orbitals of the $S = 5/2$ magnetic state. As seen in Figure 2, the second approach converges more rapidly due to better cancellation of basis-set errors. The difference of the two approach diminishes systematically as N_{KS} approaches the full planewave basis limit, as expected. Since it is highly desirable to use a downfolded basis that will converge rapidly to the full planewave basis limit, we will use the second approach in the subsequent calculations.

The results in Figure 2 show that the calculated spin gap is already in good agreement with the full planewave result at 53 basis functions. This represents only a small fraction of the full planewave basis (2488 basis functions). Similar to the result in silicon, the convergence of the spin gap to the full basis set limit is not monotonic, showing the largest deviation (~0.12 eV) at $N_{KS} = 100$, although the error in the gap is well below 0.1 eV beyond 100 basis functions. These results indicate that it is possible to construct realistic models from the downfolding approach which are much simpler than the full Hamiltonian and capable of giving quantitatively accurate results.

We next demonstrate the significant error of the standard single-projector, norm-conserving Ne-core PP as employed in many-body simulations, and how it can be removed in the current approach with little additional computational cost. The PP effects on ΔE are shown in Figure 3. The left panel compares Ne-core and He-core PP DFT calculations with PAW and with all-electron LAPW values. The results are tabulated in Table 3. The DFT calculations show that the Ne-core PP leads to an overestimation of the gap by almost 0.4 eV. By contrast, the He-core PP gap is in excellent agreement with the all-electron LAPW value. While the PAW calculation also uses a Ne-core PP, it uses two (or more) projectors per angular momentum channel and is seen to reproduce the LAPW result well. We therefore attribute the poor performance of the Ne-core norm-conserving PP not to the underlying frozen-core approximation for the Mn 2s and 2p states, but rather to the

Table 3. Accurate Determination of the Energy Gap ΔE (in eV) between the High- and Low-Spin Phases with Downfolded Hamiltonians and FC Calculations, and the Inadequacy of Single-Projector Pseudopotentials[a]

		Basis Set		Cutoff	DFT/GGA	AFQMC
Mn PP	N_e	type	M	parameter (Ry)	ΔE	ΔE
Ne-core	21	PW	2488	$E_{cut} = 100$	1.51	2.13(1)
		KS	53	$\Delta\varepsilon_{KS} = 9.6$		2.164(3)
He-core	29	PW	160046	$E_{cut} = 1600$	1.14	
		KS	57	$\Delta\varepsilon_{KS} = 9.6$		1.651(7)
He-core + FC	21	KS	53	$\Delta\varepsilon_{KS} = 9.6$		1.649(9)
AE	21	PAW	4584	$E_{cut} = 150$	1.11	
AE	29	LAPW	266	$E_{cut} = 22$	1.13	

[a]AFQMC results using Ne-core PP, He-core PP, He-core PP with FC approximation are compared. Corresponding DFT calculations are also shown to illustrate consistency. N_e is the number of electrons in the simulation cell, and M is the number of single-particle basis functions.

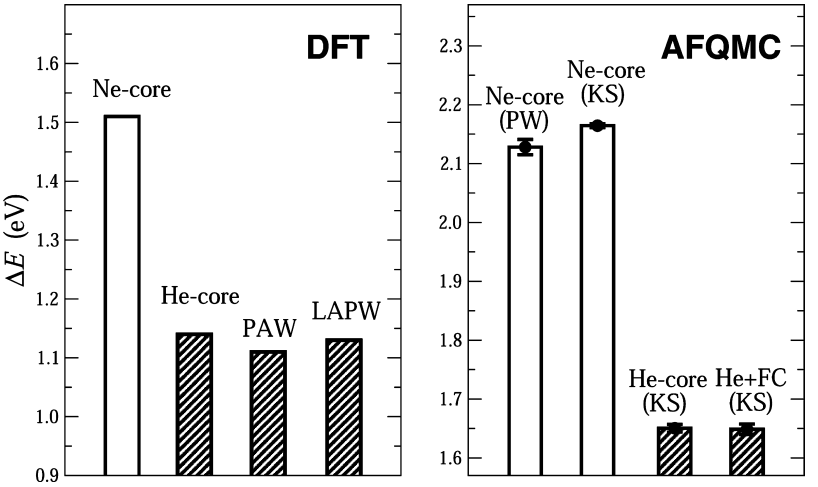

Figure 3. Calculations of the energy gap ΔE between the high- and low-spin phases in MnO. DFT results are shown on the left panel, while AFQMC results on the right. Downfolded Hamiltonians lead to accurate results in AFQMC, as seen from the comparison with the planewave calculations. The single-projector, Ne-core PP is inadequate, as illustrated at both the DFT and the QMC levels of theory. AFQMC with FC Hamiltonian (He+FC) is in excellent agreement with the "all-electron" result. Actual numerical values are presented in Table 3.

dx.doi.org/10.1021/ct4006486 | J. Chem. Theory Comput. XXXX, XXX, XXX–XXX

deficiency of its being only a single-projector PP. The excellent transferability of the He-core PP indicates that the single-projector representation is sufficient for this much harder PP.

The right panel in Figure 3 shows AFQMC results, which are consistent with the DFT trends and illustrate clearly the different aspects of the transferability issues in a many-body context. For the Ne-core PP, results are shown from both the full planewave basis and the KS basis (N_{KS} = 53, as described earlier). For the He-core PP, AFQMC results are shown for both an "all-electron" (He-core) Hamiltonian fully correlating the 2s and 2p Mn states (N_{KS} = 57), and from a FC Hamiltonian (N_{KS} = 53), where these states are frozen at the DFT level. The discrepancy in ΔE between the Ne-core PP and the He-core results increases to ∼0.5 eV in the many-body results. The excellent agreement between the two He-core results indicates the accuracy of the FC approximation in the many-body calculations. Accurate and efficient AFQMC calculations are thus achieved at a cost comparable to a Ne-core PP using the downfolded Hamiltonian and the FC approximation.

5. SUMMARY

The frozen orbital and downfolding approach described in this paper can provide significant computational savings, compared to fully correlating all the electrons in both molecular and extended systems. The key idea of identifying a physically important "active" subspace of the full Hilbert space is already inherent in the standard FC approximation used in explicitly correlated wavefunction-based many-body quantum chemistry methods. We have shown how the frozen-core (FC) approximation can be implemented in auxiliary-field quantum Monte Carlo (AFQMC). With a GTO basis set, FC AFQMC treats exactly the same Hamiltonian as standard quantum chemistry methods. This effectively eliminates the chemically inactive core degrees of freedom (and electrons) from the calculation, resulting in greatly increased computational efficiency, particularly for heavy atoms. Scalar relativity for such systems can be easily treated using the DKH approximation to the Hamiltonian. More generally, the downfolding of high-energy basis states to a physically relevant low-energy sector can greatly increase the efficiency of this approach in solid-state applications. As an example, we have shown in this paper how to effectively eliminate the error due to single-projector, norm-conserving PPs. The fact that AFQMC is an orbital-based method is the key feature that enables the partitioning and downfolding schemes described here.

The results presented in this paper are a proof of concept that the downfolding and FC approaches could greatly extend the reach of many-body calculations to larger and more-complex systems. Clearly, AFQMC applications with these approaches require further study. For example, the simple downfolding application we have described is based on a single energy cutoff. The efficiency of the method could be greatly improved by employing additional physically based criteria.

The FC approach can also be generalized to other partitioning schemes of the Hilbert space into active and inactive regions. In molecular and condensed matter physics, for example, the active region may sometimes be identified spatially, corresponding to a localized region where strong electron correlation effects affect a relatively small number of atoms, while the bulk of the system can be treated with a lower level of theory. Various theories of partitioning (see ref 2, for example) or embedding[39−43] have been developed to exploit this locality and improve computational efficiency.[44,45] AFQMC can also benefit from efficiencies derived from the use of localized orbital transformations obtained from Boys[46] or Wannier[47,48] localization.

AUTHOR INFORMATION

Corresponding Authors

*E-mail: wirawan0@gmail.com.
*E-mail: shiwei@wm.edu.
*E-mail: krakauer@wm.edu.

Notes

The authors declare no competing financial interest.

ACKNOWLEDGMENTS

This work was supported by DOE (No. DE-FG02-09ER16046), NSF (No. DMR-1006217), and ONR (Nos. N000140811235 and N000141211042). An award of computer time was provided by the Innovative and Novel Computational Impact on Theory and Experiment (INCITE) program, using resources of the Oak Ridge Leadership Computing Facility (Jaguar/Titan) at the Oak Ridge National Laboratory, which is supported by the Office of Science of the U.S. Department of Energy (under Contract No. DE-AC05-00OR22725). This research is part of the Blue Waters sustained-petascale computing project, which is supported by the National Science Foundation (Award No. OCI 07-25070) and the state of Illinois. Blue Waters is a joint effort of the University of Illinois at Urbana−Champaign and its National Center for Supercomputing Applications. We also acknowledge the computing support from the Center for Piezoelectrics by Design. The authors thank Eric J. Walter for many useful discussions, his help in generating pseudopotentials, and performing the PAW and LAPW calculations.

REFERENCES

(1) Kahn, L. R.; Baybutt, P.; Truhlar, D. G. *J. Chem. Phys.* **1976**, *65*, 3826−3853.
(2) Huzinaga, S. *J. Mol. Struct. (THEOCHEM)* **1991**, *234*, 51−73.
(3) Suewattana, M.; Purwanto, W.; Zhang, S.; Krakauer, H.; Walter, E. J. *Phys. Rev. B* **2007**, *75*, 245123.
(4) Hennig, R. G.; Wadehra, A.; Driver, K. P.; Parker, W. D.; Umrigar, C. J.; Wilkins, J. W. *Phys. Rev. B* **2010**, *82*, 014101.
(5) Sorella, S.; Casula, M.; Spanu, L.; Corso, A. D. *Phys. Rev. B* **2011**, *83*, 075119.
(6) Fracchia, F.; Amovilli, C. *Chem. Phys. Lett.* **2012**, *521*, 20−25.
(7) Kolorenč, J.; Mitas, L. *Phys. Rev. B* **2007**, *75*, 235118.
(8) Zhang, S.; Krakauer, H. *Phys. Rev. Lett.* **2003**, *90*, 136401.
(9) Al-Saidi, W. A.; Zhang, S.; Krakauer, H. *J. Chem. Phys.* **2006**, *124*, 224101.
(10) Purwanto, W.; Zhang, S.; Krakauer, H. *J. Chem. Phys.* **2009**, *130*, 094107.
(11) Purwanto, W.; Krakauer, H.; Zhang, S. *Phys. Rev. B* **2009**, *80*, 214116.
(12) Purwanto, W.; Krakauer, H.; Virgus, Y.; Zhang, S. *J. Chem. Phys.* **2011**, *135*, 164105.
(13) Ma, F.; Zhang, S.; Krakauer, H. *New J. Phys.* **2013**, *15*, 093017.
(14) Zhang, S.; Carlson, J.; Gubernatis, J. E. *Phys. Rev. B* **1997**, *55*, 7464.
(15) Purwanto, W.; Zhang, S. *Phys. Rev. E* **2004**, *70*, 056702.
(16) Valiev, M.; Bylaska, E.; Govind, N.; Kowalski, K.; Straatsma, T.; van Dam, H.; Wang, D.; Nieplocha, J.; Apra, E.; Windus, T.; de Jong, W. *Comput. Phys. Commun.* **2010**, *181*, 1477−1489.
(17) Schmidt, M. W.; Baldridge, K. K.; Boatz, J. A.; Elbert, S. T.; Gordon, M. S.; Jensen, J. H.; Koseki, S.; Matsunaga, N.; Nguyen, K. A.;

Su, S. J.; Windus, T. L.; Dupuis, M.; Mont gomery, J. A. *J. Comput. Chem.* **1993**, *14*, 1347−1363.
(18) Balabanov, N. B.; Peterson, K. A. *J. Chem. Phys.* **2005**, *123*, 064107.
(19) Douglas, M.; Kroll, N. M. *Ann. Phys.* **1974**, *82*, 89−155.
(20) Hess, B. A. *Phys. Rev. A* **1985**, *32*, 756−763.
(21) Hess, B. A. *Phys. Rev. A* **1986**, *33*, 3742−3748.
(22) Helgaker, T.; Klopper, W.; Koch, H.; Noga, J. *J. Chem. Phys.* **1997**, *106*, 9639−9646.
(23) Al-Saidi, W. A.; Zhang, S.; Krakauer, H. *J. Chem. Phys.* **2007**, *127*, 144101.
(24) Purwanto, W.; Al-Saidi, W. A.; Krakauer, H.; Zhang, S. *J. Chem. Phys.* **2008**, *128*, 114309.
(25) Beebe, N. H. F.; Linderberg, J. *Int. J. Quantum Chem.* **1977**, *12*, 683−705.
(26) Koch, H.; de Merás, A. S.; Pedersen, T. B. *J. Chem. Phys.* **2003**, *118*, 9481−9484.
(27) Aquilante, F.; Vico, L. D.; Ferré, N.; Ghigo, G.; åke Malmqvist, P.; Neogrády, P.; Pedersen, T. B.; Pitonák, M.; Reiher, M.; Roos, B. O.; Serrano-Andrés, L.; Urban, M.; Veryazov, V.; Lindh, R. *J. Comput. Chem.* **2010**, *31*, 224−247.
(28) Lin, C.; Zong, F. H.; Ceperley, D. M. *Phys. Rev. E* **2001**, *64*, 016702.
(29) Kwee, H.; Zhang, S.; Krakauer, H. *Phys. Rev. Lett.* **2008**, *100*, 126404.
(30) Ma, F.; Zhang, S.; Krakauer, H. *Phys. Rev. B* **2011**, *84*, 155130.
(31) Baldereschi, A. *Phys. Rev. B* **1973**, *7*, 5212−5215.
(32) Yoo, C. S.; Maddox, B.; Klepeis, J.-H. P.; Iota, V.; Evans, W.; McMahan, A.; Hu, M. Y.; Chow, P.; Somayazulu, M.; Häusermann, D.; Scalettar, R. T.; Pickett, W. E. *Phys. Rev. Lett.* **2005**, *94*, 115502.
(33) Kondo, T.; Yagi, T.; Syono, Y.; Noguchi, Y.; Atou, T.; Kikegawa, T.; Shimomura, O. *J. Appl. Phys.* **2000**, *87*, 4153−4159.
(34) Kasinathan, D.; Kuneš, J.; Koepernik, K.; Diaconu, C. V.; Martin, R. L.; Prodan, I. D.; Scuseria, G. E.; Spaldin, N.; Petit, L.; Schulthess, T. C.; Pickett, W. E. *Phys. Rev. B* **2006**, *74*, 195110.
(35) Gonze, X.; Beuken, J.-M.; Caracas, R.; Detraux, F.; Fuchs, M.; Rignanese, G.-M.; Sindic, L.; Verstraete, M.; Zerah, G.; Jollet, F.; Torrent, M.; Roy, A.; Mikami, M.; Ghosez, P.; Raty, J.-Y.; Alla, D. *Comput. Mater. Sci.* **2002**, *25*, 478 (program available at http://www.abinit.org).
(36) Giannozzi, P.; Baroni, S.; Bonini, N.; Calandra, M.; Car, R.; Cavazzoni, C.; Ceresoli, D.; Chiarotti, G. L.; Cococcioni, M.; Dabo, I.; Dal Corso, A.; de Gironcoli, S.; Fabris, S.; Fratesi, G.; Gebauer, R.; Gerstmann, U.; Gougoussis, C.; Kokalj, A.; Lazzeri, M.; Martin-Samos, L.; Marzari, N.; Mauri, F.; Mazzarello, R.; Paolini, S.; Pasquarello, A.; Paulatto, L.; Sbraccia, C.; Scandolo, S.; Sclauzero, G.; Seitsonen, A. P.; Smogunov, A.; Umari, P.; Wentz- covitch, R. M. *J. Phys.: Condens. Matter* **2009**, *21*, 395502.
(37) The Elk full-potential linearized augmented-plane wave, available at http://elk.sorceforge.net (accessed May 1, 2011).
(38) The OPIUM project, available at http://opium.sorcef orge.net (accessed May 2, 2012).
(39) Svensson, M.; Humbel, S.; Froese, R. D. J.; Matsubara, T.; Sieber, S.; Morokuma, K. J. *Phys. Chem.* **1996**, *100*, 19357−19363.
(40) Govind, N.; Wang, Y. A.; Carter, E. A. *J. Chem. Phys.* **1999**, *110*, 7677−7688.
(41) Huang, P.; Carter, E. A. *J. Chem. Phys.* **2006**, *125*, 084102.
(42) Huang, P.; Carter, E. A. *Annu. Rev. Phys. Chem.* **2008**, *59*, 261−290 (and the references therein)..
(43) Elliott, P.; Burke, K.; Cohen, M. H.; Wasserman, A. *Phys. Rev. A* **2010**, *82*, 024501.
(44) Knizia, G.; Chan, G. K.-L. *J. Chem. Theory Comput.* **2013**, *9*, 1428−1432.
(45) Beran, G. J. O.; Hirata, S. *Phys. Chem. Chem. Phys.* **2012**, *14*, 7559−7561.
(46) Boys, S. F. *Rev. Mod. Phys.* **1960**, *32*, 296−299.
(47) Wannier, G. H. *Phys. Rev.* **1937**, *52*, 191−197.
(48) Marzari, N.; Vanderbilt, D. *Phys. Rev. B* **1997**, *56*, 12847−12865.